Electronic Supplementary Material (ESI) for Journal of Materials Chemistry A.

SUPPLEMENTARY INFORMATION

Insights into the active nickel centers embedded in graphitic carbon nitride for the oxygen evolution reaction

Nicolò Rossetti, Aldo Ugolotti, Claudio Cometto, Verónica Celorrio, Goran Dražić, Cristiana Di Valentin*, Laura Calvillo*

Corresponding authors: cristiana.divalentin@unimib.it; laura.calvillolamana@unipd.it

Numerical screening of different pristine CN structures.

In order to identify the most probable melamine-based CN structure synthesized in the samples, we performed a computational study of several CN polymorphs. We considered different degrees of polymerization, different arrangements of the monomers and different dimensionalities, i.e. two-dimensional (2D) or bulk. All the models we optimized are shown in Figure S1a-f. For each of these structures, we carried out a characterization based on the simulation of both the XRD pattern and the N 1s XPS spectrum, which are reported in Figures S1g and S1h, respectively, in order to find the configuration with the best agreement with the actual CN samples.

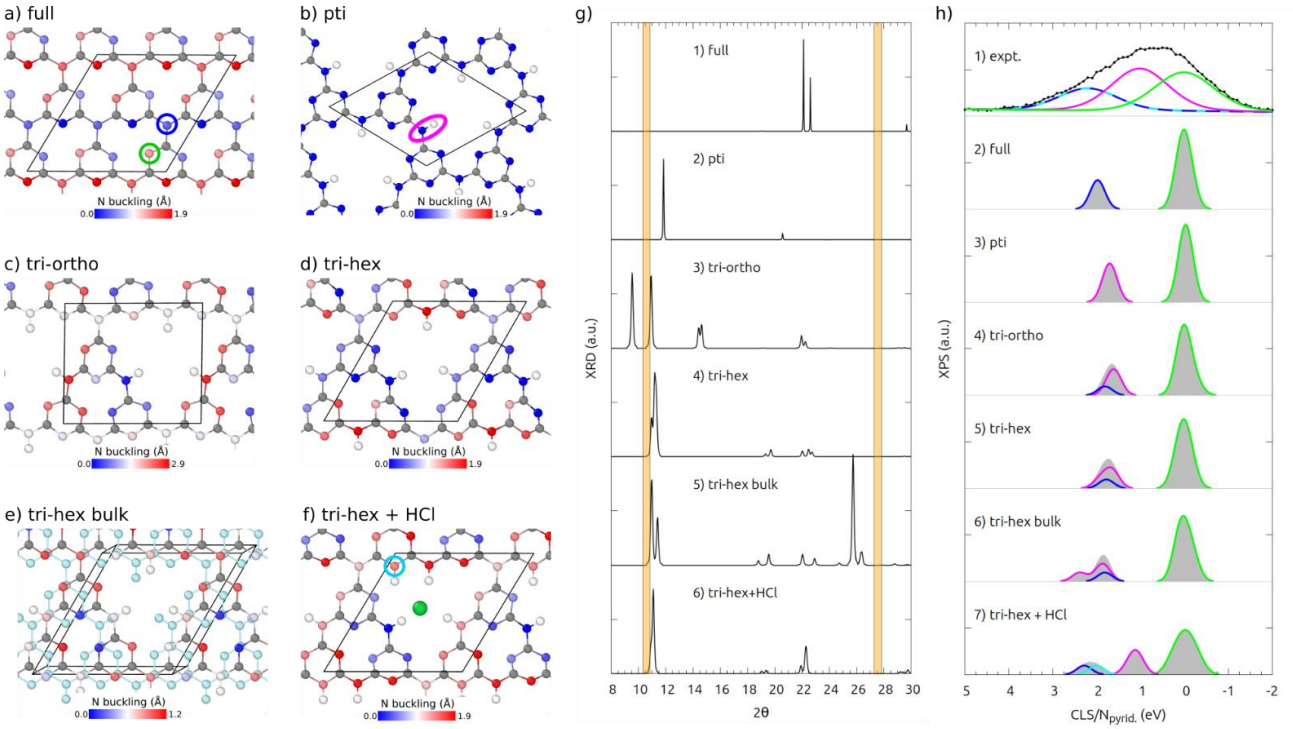

Figure S1. Panels a-f: top view of different CN structures: (a) fully polymerized 2D s-triazine; (b) 2D poly(triazine imide); (c) 2D triazine-based orthogonal; (d) 2D triazine-based hexagonal; (e) heterostructure (bulk) of triazine-based hexagonal; (f) 2D HCl-decorated triazine-based hexagonal. The N atoms of each structure are colored to show the corrugation of the geometry. The color scale is reported at the bottom of all panels. The C, H and Cl atoms are shown with grey, white and green spheres, respectively. On the panels, different N types are marked through colored circles: pyridinic N (green), amino N (magenta), graphitic N (blue) and protonated pyridinic N (cyan). In panel e), the light azure atoms shown the 2nd layer of the heterostructure. Panel g: comparison between the simulated XRD patterns and the experimental peaks (orange lines). Panel h: comparison between the simulated and the experimental XPS spectra. In simulated spectra, the contributions of the different N atoms (marked in panels a-f) are shown, as well as the components obtained by fitting the experimental data (black line).

In the case of the XRD patterns (Figure S1g), although the agreement of the position of the calculated peaks with the experimental ones in the low-angles region is not extremely satisfactory, it is still possible to identify the best structure of the melamine polymer to use as our model, which is the one with partially condensed *s*-triazine units, which we label tri-hex (Figure S1d). The XPS results (Figure S1h), however, show that no model is able to reproduce the peak with a core level shift (CLS) of c.a. +1 eV with respect to that of the pyridine N atoms, corresponding to a binding energy of c.a. 399.5 eV. Therefore, we concluded that the sample still contains traces of H^+ and Cl^- ions from the synthesis: we re-optimized the coordinates of the tri-hex structure including an H atom adsorbed on the border

of a large pocket and a Cl atom electrostatically interacting with pyridinic N atoms of the same pocket. This structure is shown in Figure S1f. For this new model, we also optimized the lattice parameters of the supercell. However, the periodicity of the two-dimensional layer is similar to that of the pristine tri-hex CN model, hence their XRD patterns (Figure S1g4-6) do not differ much. In the simulated XPS spectrum (Figure S1h7), instead, a new peak appears, with a CLS of c.a. +1 eV, which is in good agreement with the experimental result. Such an additional feature is originated by the redshift of the amino N atoms.

Additional TEM and HRTEM images

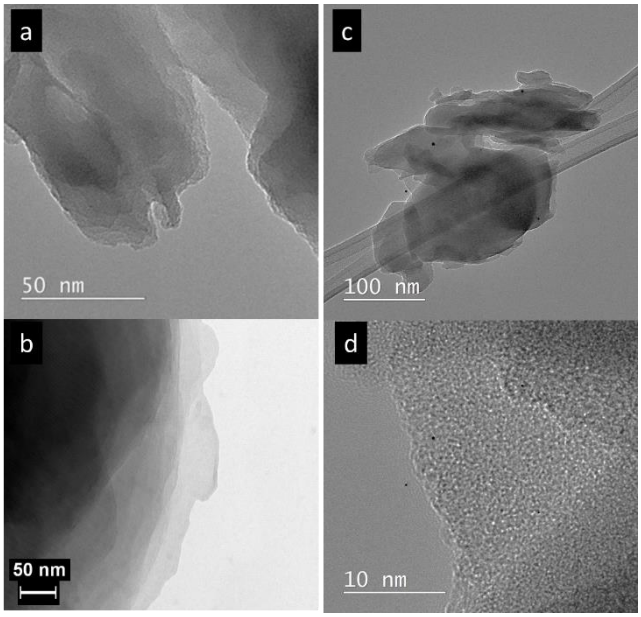

Figure S2. Additional TEM images of (a, b) CN and (c, d,) Ni-CN (0.2).

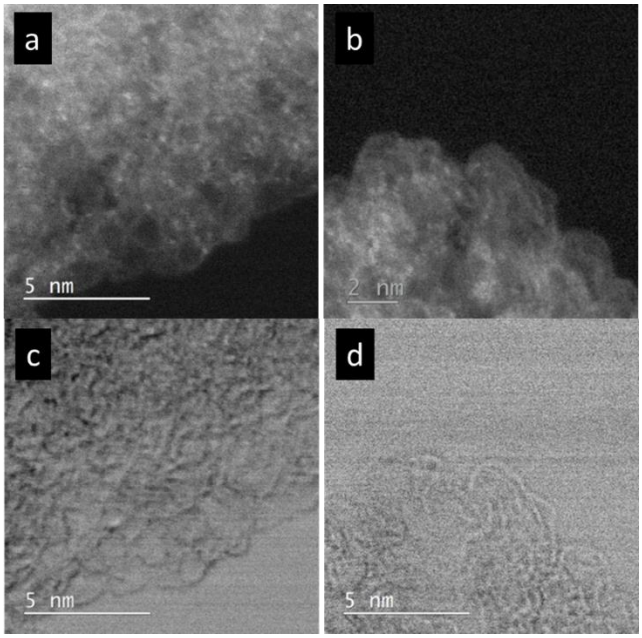

Figure S3. Additional STEM images of Ni-CN (0.2): (a, b) dark-field and (c, d) bright-field.

Additional XPS results

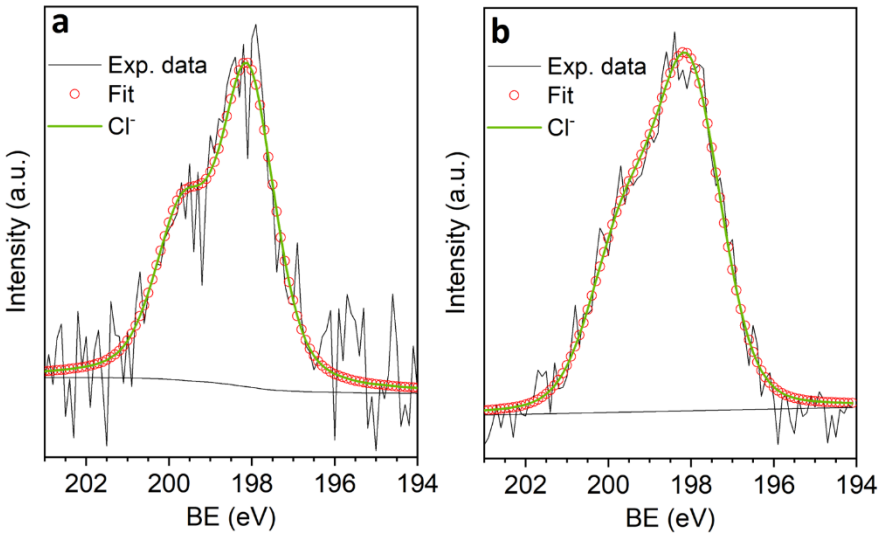

Figure S4. Experimental Cl 2p XPS region for (a) CN and (b) Ni-CN(0.2), and its separation into single chemical components.

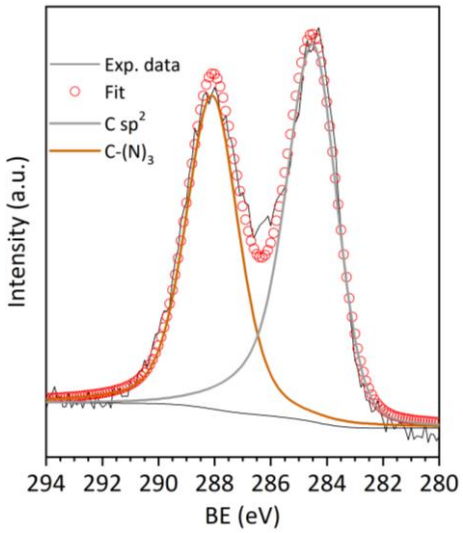

Figure S5. Experimental C 1s XPS region for Ni-CN(0.2), and its corresponding separation into chemical shifted components.

Table S1. Analysis of the C 1s XPS region. For each component, the binding energy and the percentage (at.%) are reported.

Sample	C-C	C-$(N)_3$
CN	285.0 eV 57.8%	287.8 eV 42.2%
Ni-CN	284.5 eV 56.3%	288.1 eV 43.7%

Table S2. Analysis of the N 1s XPS region. For each component, the binding energy and the percentage (at. %) are reported.

Sample	C-N=C	$(C)_2$-NH/ Ni-N	$(C)_3$-N/ $(C)_2$-NH
CN	398.3 eV 37.9%	399.3 eV 40.0%	400.5 eV 22.1%
Ni-CN	398.2 eV 30.5%	399.2 eV 45.7%	400.5 eV 23.8%

Numerical screening of different Ni-decorated CN structures.

To define the best Ni-CN model, we considered the tri-hex structure described above, and we optimized its coordinates after placing one additional Ni and two additional Cl atoms within an enlarged 2x2 supercell. We relaxed the atomic coordinates only, keeping fixed the supercell structure; this constraint should mimic the experimental setup with a low concentration of Ni atoms, as observed in actual samples.

Since 2D tri-hex structure is a porous one, there are two different pockets where the Ni adatoms can be placed: a small one and a large one; therefore, we optimized two models, which we report in Figure S6a and b and that we label model1 and model2, respectively. We calculated the $NiCl_2$ adsorption energy as $\Delta E=E_{NiCN}-E_{CN}-E_{NiCl2}$; for the two models ΔE(model1) = -1.1 eV and ΔE(model2) = -2.5 eV. Even though model2 seems the best candidate model, the Ni adatom within its structure interacts directly with two pyridinic N atoms only (and the Cl one): this result does not agree with EXAFS data, where a coordination 4 can be inferred. Since the metalation step is performed using hydrated salts, we considered that Ni atoms might have retained a number of water molecules. We verified our hypothesis by optimizing model2 including two additional water molecules, placed azimuthally to the Ni-N bonds plane, as shown in Figure S6c. The new model is in better agreement with the previous model2 one, since coordination of Ni atom seems properly described. Our Ni-CN models do not include additional H atoms, differently from the case of pristine CN. We assumed that the experimental spectrum measured for actual Ni-CN samples is the result of the superposition of that we calculated for the model2+H_2O structure and that we calculated for the tri-hex+HCl one. Additionally, the weak H_2O-Ni interaction is not expected to significantly alter the chemical environment around the pyridine N atoms, therefore we deemed the XPS spectrum of model2+H_2O to be similar to that we calculated for the model2.

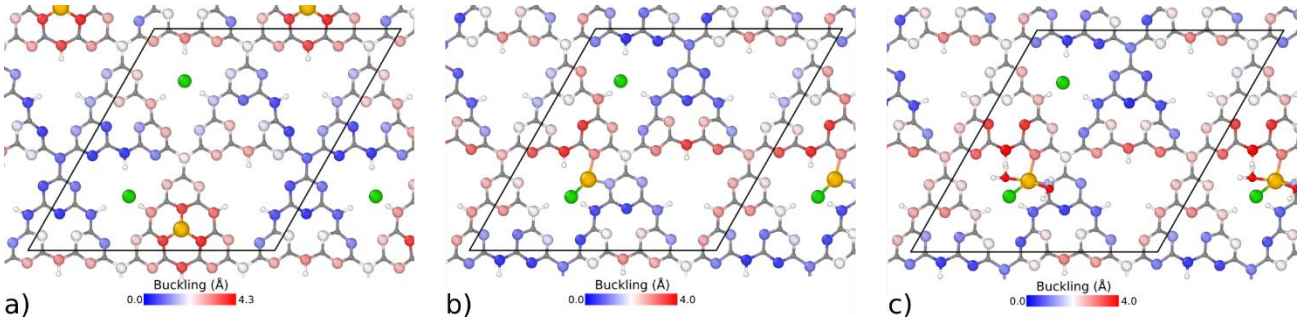

Figure S6. Optimized models of Ni-CN, with Ni adatom (orange sphere) on top of a small pocket (panel a, model 1) and within the large pocket (panel b, model 2), also with addition of two water molecules (panel c, model 2') The color of N atoms represents the corrugation of the structure: the color scale is reported at the bottom of each panel. C, H and Cl atoms are represented by grey, white and green spheres.

Additional EXAFS results of the as-prepared samples

Table S3. Structural parameters obtained for the two fresh Ni-CN samples from fitting the Ni K edge FT EXAFS data (k = 2.3 – 11; R = 1.0 – 2.3 Å). CN is the coordination number, R is the interatomic distance, and σ^2 is the Debye-Waller factor.

Sample	Shell	CN	R (Å)	σ^2 x 10^4 (Å^2)	E_0 (eV)	R_f	S_0^2
Ni-CN(0.05)	Ni-N	2.0	2.04 ± 0.04	22 ± 13	-0.400	0.010	1.1 ± 0.32
	Ni-O	2.0	2.14 ± 0.05	110 ± 14			
Ni-CN(0.3)	Ni-N	2.0	2.01 ± 0.05	79 ± 8	-2.06	0.017	1.1 ± 0.18
	Ni-O	2.0	2.12 ± 0.04	98 ± 14			

RRDE experiment

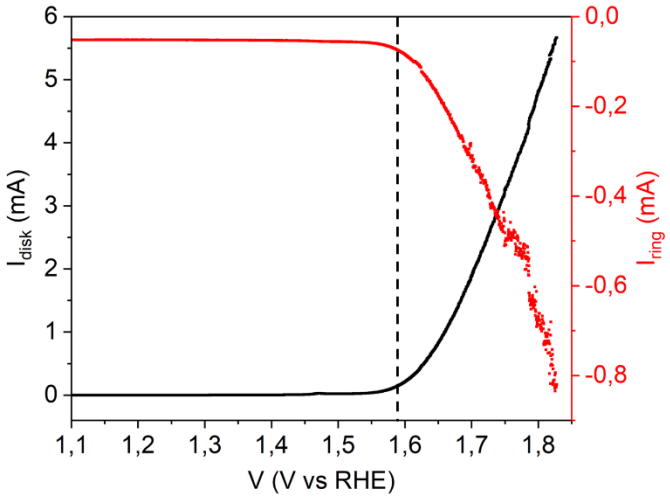

Figure S7. Polarization curve at 1600 r.p.m and simultaneous oxygen detection current at the Pt ring electrode (V_{ring}=-0.8 V vs Hg/HgO) for Ni-CN(0.2) in N_2-saturated 0.1 M KOH.

Elemental analysis and ICP-MS results

Table S4. Elemental Analysis and ICP-MS quantification.

Sample	N	C	H	Ni (% w/w)
CN	42.09 ± 0.5	33.18 ± 0.5	4.33 ± 0.2	---
Ni-CN(0.05)	40.72 ± 0.5	31.48 ± 0.5	4.26 ± 0.2	0.42 ± 0.05
Ni-CN(0.2)	41.58 ± 0.5	32.32 ± 0.5	3.59 ± 0.2	0.88 ± 0.05
Ni-CN(0.3)	41.28 ± 0.5	31.85 ± 0.5	3.23 ± 0.2	0.99 ± 0.05
Ni-CN(0.4)	41.31 ± 0.5	31.35 ± 0.5	2.10 ± 0.2	1.01 ± 0.05

Post-AAT characterization

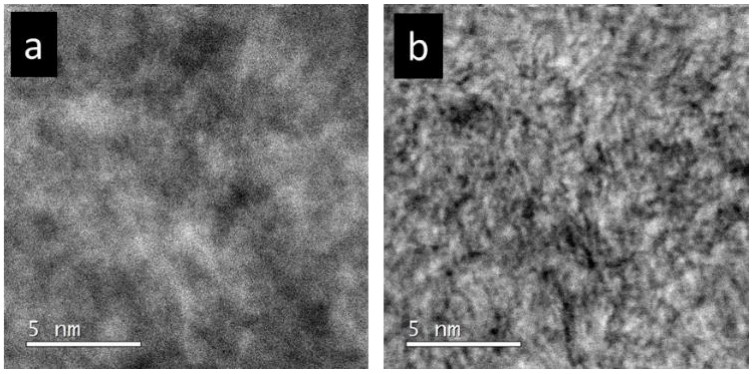

Figure S8. (a) HAADF-STEM, and (b) BF-STEM image of aged Ni-CN (0.2).

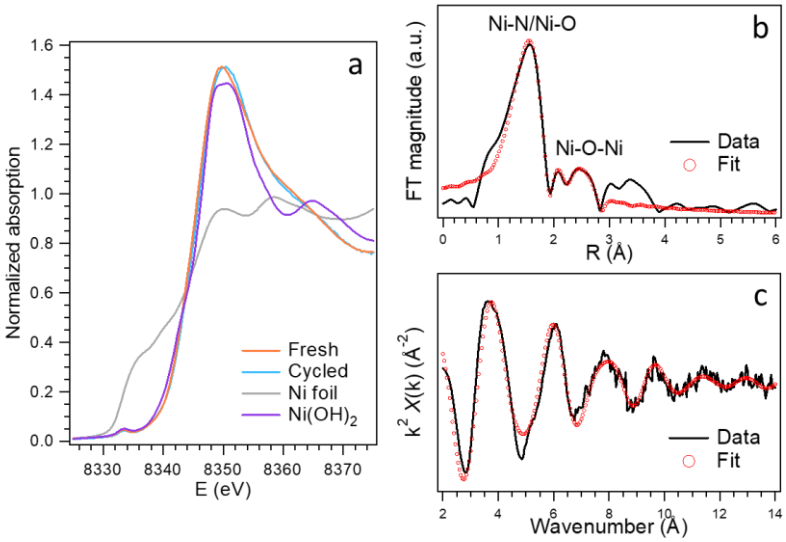

Figure S9. (a) XANES spectra at the Ni K edge of the fresh and aged Ni-CN(0.2) sample; (b) phase-uncorrected FT EXAFS spectrum and corresponding fit; and (c) k^2 weighted experimental data and fit at the Ni K edge for the cycle Ni-CN(0.2) sample.

Table S5. Structural parameters obtained for the aged Ni-CN(0.2) sample from fitting the Ni K edge FT EXAFS data (k = 2.3 – 13; R = 1.0 – 3.2 Å). CN is the coordination number, R is the interatomic distance, and σ^2 is the Debye-Waller factor.

Shell	CN	R (Å)	σ^2 x 10^4 (Å^2)	E_0 (eV)	R_f	S_0^2
Ni-N_1	2.0	1.98 ± 0.03	55 ± 13	-2.96	0.011	1.3 ± 0.31
Ni-O	2.0	2.08 ± 0.03	45 ± 6			
Ni-C	2.0	2.76 ± 0.03	148 ± 93			
Ni-N_2	2.0	2.96 ± 0.14	156 ± 68			
Ni-Ni	1.0	3.06 ± 0.07	104 ± 92			

Steady state potential measurements

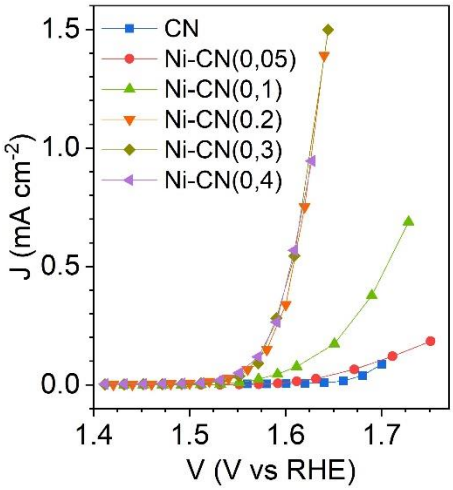

Figure S10. Steady state current densities at different potentials (100% iR drop corrected).